Performance of bolted steel-beam to CFST-column joints using stiffened angles in column-removal scenario

Shan Gao[a,b]*, Man Xu[c], Feng Fu[d], Lanhui Guo[e]

[a] Shaanxi Key Laboratory of safety and durability of concrete structures, Xijing University, Xi'an 710123, China

[b] Postdoctoral Station of Civil Engineering, Chongqing University, Chongqing 400030, China

[c] School of Civil Engineering, Northeast Forestry University, Harbin 150090, China

[d] School of Mathematics, Computer Science & Engineering, University of London, London, EC1V0HB, UK

[e] School of Civil Engineering, Harbin Institute of Technology, Harbin 150090, China

Abstract: This paper presents three experimental investigations on the performance of steel-beam to CFST-column joints using stiffened angle, long bolts and fin plate under a middle column removal scenario. Three specimens were designed and tested. The failure modes and catenary action are investigated in detail. The test results show that increasing the angle plate thickness at the joint could not only improve its performance significantly, but also trigger an early formation of catenary action. Increasing the length of short-limb had influence on the deformation ability of the proposed joint, rather than the load capacity. The buckling of stiffeners could prevent the brittle failure of the joints. With the contribution of catenary action, the joint shows much higher rotation capacities than that required in DoD design guidance. The initial stiffness of the joint was calculated using an analytical model with consideration of bolt pretension. Good agreement to the test results is achieved. A numerical analysis is also carried out, whose results show that adding additional row of bolts would improve the redundancy of the joint under column loss. An equivalent dynamic response evaluation of the joints was also performed. The results show that dynamic amplification coefficient should be worked out considering catenary action under large deformation.

Keywords: CFST; progressive collapse; stiffened angle bolted joints; catenary action; component method

1. Introduction

Progressive collapse of structures may be triggered by the loss of columns. In the scenario of column-removal, vertical loads on the structure would be redistributed to the beams connected to the removed column [1-2]. With the increase of vertical deformation, the load-carrying mechanism in the damaged structure will transform from plastic hinge action to catenary action as shown in Fig. 1. The performance of beam-column joints under the combination of bending moment and tensional force in the scenario of column removal is a key factor in the prevention of progressive collapse. However, in traditional design, beam-column joints are designed to carry only bending moments.

In order for the joint to behave properly in such conditions, the rotation capacity of the joints should be fulfilled to mobilize catenary action while the redundancy of the joints is required in order to avoid brittle damages and to absorb energy. Therefore, the features of joint behavior are identified as follows: Under plastic hinge action, the reverse load-carrying capacity of the joint is required in where the joints at the damaged column are under sagging moment rather than under hogging moment; During the transition of load-carrying mechanism, the joints at the damaged column and the adjacent columns should be capable of carrying the particular load sequences involving bending moments and axial forces; After tensile catenary action is triggered on the beams, the joints would undergo large deformation without any significant reduction in strength. These demands are rarely met in normal design of joint, but crucial in the design of resisting progressive collapse. Therefore it requires further investigation through experimental tests. Several studies have been performed on the behavior of connections under the combination of axial loads and moment [3-5]. However, those studies did not study in detail on the effect of the axial force to the performance of joints under column removal.

The configuration of special blind bolts or intermediate components (such as reverse channel) are used in practice to connect steel beam to concrete-filled steel tubular (CFST) column or hollow section column[6]. These configurations of connections could overcome the difficulty of placing bolts into the closed-profile column. However, the stiffness and resistance of those types of joints are low in bending. Meanwhile, the in-filled concrete has limited contribution to the bending strength of joint, since the column wall is directly under flexural action when the bolts are under tension, as shown in Fig. 2 (a). Hence, long bolts throughout the column are proposed to connect steel beam to CFST column or hollow section column recently. For hollow section columns, care must be taken when installing long bolts into the thin wall of the hollow section column so as to prevent distortion of the sidewalls as shown in Fig. 2 (b). With the existence of interior filled concrete, this configuration of connection becomes more practical [7-8]. The core concrete acts together with column wall when pretension loads are applied on bolts, as shown in Fig. 2 (c). It should be mentioned that the steel beam-CFST column joint with long bolts may be more

vulnerable than the other two mentioned solutions, from the perspective of anti-collapse mechanism. Once the long bolts fracture, the connections at both sides of the column would fail at the same time. In that case, the flexible components should be used in the connection to avoid the fracture of long bolts, such as angle steel or endplate.

In the past decades, many studies have been conducted on the bending behavior or seismic behavior of steel-beam to CFST-column. Wang and Chen [9] conducted a test on blind bolted extended end plate joints to CFST columns under bending moment. The results showed that the performance of tested connections could meet the demands of anti-seismic design. A model to predict the stiffness and resistance of bolted joints based on component method was proposed by Thai and Uy [10]. Huang et al. [11] developed a formula to calculate the resistance of CFST joints based on Eurocode 3 (EC3). The references about the study on static and seismic behavior of CFST column joints provide a basis to understand the behavior of the joint under bending moment which plays a key role at the early stage of column-removal and the failure modes of traditional CFST column joints, also to improve the configuration of traditional connection. It should be mentioned that component method needs to be further developed to enable the design of the connection with long bolts.

Regarding the behavior of joints under column-removal scenario, the joints connecting steel-beam to steel-column and to CFST-column are both studied. Khandelwal and EI-Tawil [12] used finite-element model to study some critical parameters that affect the catenary action in steel structures. Demonceau and Jaspart [13] discussed the effects of membrane forces on the behavior of joints. Sadek et al. [14] carried out an experiment to assess the behavior of steel joint under column removal. A simplified finite element model was established to represent the behavior of the joints. Yang and Tan [15] carried out a series tests of bolted steel joints under middle column loss. The results showed that the rotation capacities of the joints were much higher than the recommended values in standards. Li et al. [16] revealed two failure modes of CFST column connections with outer-ring in the progressive collapse. Stylianidis and Nethercot [17] developed a mechanical approach to describe the performance of joints in progressive collapse analysis. Six flush endplate joints were tested by Gao et al. [18] to investigate the influence of tensional load on the bending performance of joints in progressive collapse of frame structures. Daneshvar and Driver [19] proposed a new method to predict the performance of fin plate joints in anti-collapse design. Gong [20] developed a mathematical model based on a component-based spring model which was validated against the experimental results.

So far, most of documented progressive collapse analysis focuses on the bolt-welded steel and composite joints whilst some investigations have been performed to reveal the behaviour of steel beam to CFST columns with ring plates in the event of progressive collapse. Very limited researches on the performance of the bolted steel-beam to

CFST-column connections using stiffened angle under column loss have been conducted, especially with the one using long bolts. In this paper, three steel-beam to CFST-column joint with stiffened angle, long bolts and fin plate were tested in the scenario of middle column removal. The failure modes, catenary action development and deformation ability of joints were discussed in detail. In addition, numerical analysis was conducted. Beside the experimental and numerical analysis, the equivalence dynamic response and progressive collapse capacity of the joints were also evaluated.

2. Experimental program

2.1. Design and fabrication of specimen

As shown in Fig. 3, in this investigation, it is assumed that one bottom internal column of the frame structure was destroyed, and the remaining structure after removing the middle column is regarded as the investigation object. After the removal of the middle column, the internal forces and deflection of the middle and end connections are anti-symmetric. Therefore the inflection points of the middle two bays where the column was removed were located in the middle span on both sides during the deflection process. The remaining bays are literally acting as fixed supports to the middle two bays. Therefore, the middle joint with half span beam on the both sides was extracted from the frame, and the pin supported at both end of the beams. In that case, the extracted sub-structure is used as the tested specimen.

As shown in Fig. 4(a), a steel beam-CFST column connection using stiffened angle, fin plate joints and long bolts was developed in this study. The fin plate was welded on the wall of steel tube. The web of steel-beam was connected with the fin plate using high-strength shear bolts. The flanges of the steel beam was connected to CFST column by angles. The stiffeners were welded to the angles to ensure the rigid connection of the joints. In order to ensure the axial tension of the joints in progressive collapse, long bolts were used to connect the column and angles.

Three 2/3 scaled specimens, named as WZ1, WZ2 and WZ3 respectively, were designed for the test, as shown in Fig. 4. The design of steel beams and CFST columns in the prototype structure were in accordance to GB50017-2017 [21] for steel structures and GB50936-2014 [22] for CFST structures respectively. The design of angles and bolts in the connections was based on GB50017-2017 [21] and EC 3 [23]. However, no guidance for the design of the stiffners at the angle was available in these standards. Thus it is supposed that the thickness of the stiffners was idential to that of the angle.

The section size of steel beam and tube was 244×175×11×7 and 300×300×12 respectively (overall depth(d) × flange width(b_f)× web thickness(t_w)× flange thickness(t_f)). The distance between two hinge supports of the specimens was 4000 mm, and the length of the specimens was 3600 mm. The long-limb length of the angle was 200 mm in the specimens, The short-limb length and the thickness of the angle were varied as listed in Table 1. 10.9 Grade M20 bolts were used for long bolts and shear bolts. The pretension force on bolts were 155 kN following the Chinese code GB50017-2017 [21]. The detailed dimensions of angles in the specimens were shown in Fig. 4(b).

2.2. Material properties

The cubes for determination of the strength and the cylinders for determination of the Young's modulus of the concrete used in the specimens were tested. The average strength and Young's modulus of concrete was 40.6 MPa and 3.2×10^4 MPa, respectively. The mechanical properties of steel components are shown in Table 2, where f_y,f_u, E_s and ε_u stand for yield strength, tensile strength, Young's modulus and ultimate strain of steel respectively.

2.3. Experimental setup

The test rigs are shown in Fig. 5. Hydraulic actuator control system was used to control vertical loading. Horizontal restraint to the specimen was provided by reaction wall and reaction frame as shown in Fig. 5(a). In order to restrain the out-plane deformation of the column during the loading process, a restraint device shown in Fig.5(c) was installed on both sides of the specimen. An in-plane restraint device shown in Fig. 5 (d) was also installed on both ends of the column to keep the column vertical during the loading process.

The vertical load was applied at the top of the specimen through displacement-controlled method achieved by the actuator with a rate of 6 mm/min. According to the research in Ref. [13], service loads which have little effect on the progressive collapse performance of joint under large vertical deformation, were not considered in the test. If a more than 20% drop is noticed for the vertical load recorded from the load cell, as well as the failure of stiffened angle part, such as bolt fracture, severe stiffener buckling, angle fracture and stiffener fracture, et al., are observed, the test would be terminated. With the contribution of the stiffeneres, the angle fracture is not supposed to happen, according to Ref. [15] and Ref. [20]. Instead, stiffener buckling and bolt failure are the most expected failure modes in the test.

The thrust force at the reaction was measured by load cells mounted inside the reaction frame as shown in Fig. 6. An extra support was used below the hinge beside the reaction frame to accommodate the extra shear force in the

screws connected the reaction frame and load cells. Two rollers were used at the support to serve as sliding supports, so that the thrust force in the beam could be effectively transferred to load cells. The other side of the frame was pin connected to the reaction wall.

The behavior of the specimen was measured and recorded during the test. Strain gauges were placed on four cross-sections of each beam as shown in Fig. 7(a). Linear variable displacement transducers (LVDTs) No. 1 to No. 6 were placed to record the vertical displacement of beams. Horizontal LVDT No.7 and No. 8 were placed to record the unexpected in-plane displacement of the column during the loading process, even though the in-plane restraint device had been set on the column as shown in Fig. 5 (d). The distribution of LVDTs is shown in Fig. 7(b). It should be mentioned that the deformation of bottom stiffened angles is not monitored by LVDTs, due to the difficulties in placing LVDTs on stiffened angles. The gap between angle and column flange is recorded by measurement ruler. Since the vertical load-displacement response of the joint is more concerned in this study, the specific influence of angle deformation on the anti-collapse behavior of the joint is not discussed in detail. The tests on the mechanical behavior of stiffened angle connection under tension are ongoing and would be discussed in the future studies.

3. Experimental results and discussions

3.1. Test on Specimen WZ1

Before the vertical displacement reached 25 mm, the specimen remained in elastic. When the vertical displacement reached 70 mm, 4 mm gap between the flange of column and the short-limb of bottom angle was observed which was gradually widened with the increase of the displacement. As shown in Fig. 8 (a), the short-limb of bottom angle deformed significantly. The stiffener of top angle buckled severely when the vertical displacement arrived at 210 mm, as shown in Fig. 8(b). At 220 mm, the bolts connecting column flange and short-limb of bottom angle were pulled out from the short-limb though the bolt holes which were partially fractured at the time, as shown in Fig. 8(c). Then the loading was terminated. The photo of the specimen after loading was shown in Fig. 8(d).

Fig. 9(a) illustrates the vertical force-displacement curves of WZ1. Total vertical load P is resisted by two load resistance mechanisms, namely the load carried by bending action (P_{BA}) and by catenary action (P_{CA}), as expressed by Eq. (1):

$$P = P_{BA} + P_{CA} \qquad (1)$$

The load P_{CA} could be expressed by the axial force N in beams and the rotation θ of joint:

$$P_{CA} = 2N\sin\theta \qquad (2)$$

The axial force in beams was recorded by using the load cells as shown in Fig. (6), or be calculated by the strain of steel beam, as expressed in Eq. (3):

$$N = E_s A_b (\sum_{i=1}^{n} \varepsilon_i) / n \qquad (3)$$

where E_s stands for elastic modulus of steel, A_b for the area of steel beam and ε_i for the strain obtained from the ith strain gauge at the beam section.

Fig. 9 (b) shows the axial force v.s. vertical displacement curve of left side beam. The axial load was obtained directly from the load cells. It should be mentioned that there would be little difference between the force obtained from load cell and that calculated using section strain readings. Meanwhile, the bending moment of left side connection carried by bending action P_{BA} is shown in Fig. 9(c). Fig. 9(d) shows the moment-axial force relationship of joint.

As shown in Fig. 9, the load on WZ1 was sustained only by bending action at first. Catenary action was not fully mobilized until the vertical displacement reached 120 mm. After that, catenary action in the joint started to carry vertical load until the bolts were pulled out of the angle completely when the test was terminated. Before the load resistance of WZ1 began to decrease, catenary action resisted 20 percent of total load. As shown in Fig. 9(d), the bending moment did not decrease remarkable with the increase of axial force before it reached 75 kN.

3.2. Test on Specimen WZ2

In this test, when the vertical displacement reached 89 mm, 3 mm gap between the flange of column and the short-limb of bottom angle was observed, which was slowly widened with the increase of the displacement. The deformation of the short-limb of bottom angle was shown in Fig. 10(a), when the vertical displacement had arrived at 169 mm. The gap between bottom beam flange and long-limb was observed at vertical displacement of 259 mm as shown in Fig. 10(b). A slightly buckling at top stiffeners occurred at vertical displacement of 269 mm. The bolts connecting column flange and short-limb of bottom angle were pulled out from the short-limb at the vertical displacement of 309 mm as shown in Fig. 10(c). After then the loading procedure was terminated. The specimen after loading was shown in Fig. 10(d).

As shown in Fig. 11, the load on WZ2 was sustained only by bending action at first. After the vertical displacement reached 70 mm, catenary action got involved in carrying load. After then, the load was sustained by both bending and catenary action. When the maximum moment capacity was achieved, the bending action stepped

down. However, it is observed that the total load was still increasing significantly as a result of catenary action involvement. Before the resistance of the specimen began to decrease, catenary action resisted nearly 40 percent of total load. As shown in Fig. 11(d), it is unexpected that the bending moment increased remarkably with the increase of axial force before it reached 225 kN, since a contradictory conclusion had been drawn in Ref. [13] and Ref. [18].

3.3. Test on Specimen WZ3

In this test, before the vertical displacement reached 25 mm, the specimen remained elastic. When the vertical displacement arrived at 100 mm, the buckling was observed on the top stiffeners at angles. When the vertical displacement reached 185 mm, the gap between bottom beam flange and column flange was 22 mm, meanwhile the stiffeners at top angle buckled severely, as shown in Fig. 12(a-b). The bolts connecting column flange and short-limb of bottom angle were pulled out from the short-limb at the vertical displacement of 255 mm as illustrated in Fig. 12(c). After then, the loading procedure was terminated due to the loss of bearing capacity of the specimen. The specimen after loading was shown in Fig. 12(d).

As shown in Fig. 13, the total applied load on WZ3 was sustained by bending action in initial stage. When the vertical displacement arrived at 130 mm, the load carried by bending action decreased significantly as soon as catenary action started to kick in. Even that, the total load continued to increase due to catenary action. Before the resistance of joint began to decrease, catenary action took almost 40 percent of total load. As shown in Fig. 13(d), the bending moment decreased remarkable once the axial force began to increase.

3.4. Strain and deformation analysis

It is found that, the strain distribution and deflection of the steel beams in three specimens were similar. The results of specimen WZ1 was taken as example to analyze the transition of load-bearing mechanism from bending action to catenary action.

Fig. 14(a) shows the strain distribution on steel beam of specimen WZ1. It could be seen that the strain on bottom flange continued to increase until the load capacity of WZ1 began to decrease at 180 mm. The compressive strain on top flange increased with the increase of vertical displacement before catenary action got involved in load-bearing at 120 mm. After then, compressive strain on top flange began to decrease in tensile force. It should be noticed that the steel beam section was in elastic in the whole loading procedure which indicates that the deformation of the specimen occurred in the connection part.

Fig. 14(b) shows the beam displacement profiles of specimen WZ1. It can be seen that before the formation of plastic hinge, the joint deformed as a simply-supported beam. When the load exceeded 97 kN, the beam displacement profile could be close to a straight line. It indicates that lumped plastic hinges formed at the connections.

3.5. Comparison of the specimens

The experimental results from the three specimens are summarized in Table 3 and Fig. 15. Fig. 15 (a) shows the comparison of vertical force–middle column displacement curves of three specimens. It could be seen that the load capacity of specimen WZ2 was improved significantly due to increasing the angle thickness. The load capacity of specimen WZ3 was almost the same as that of specimen WZ1, whilst the deformation ability of specimen WZ3 was better than that of specimen WZ1. It indicates that increasing the length of angle short-limb has influence on the deformation ability of the proposed joint, rather than the load capacity. As shown in Fig. 16, the effective stress area of stiffeners at the angles could be simplified as a set of strips. When the joint carries the loads, the strips in compression would buckle progressively while the strips in tensile would transfer internal force to short-limb. When the short-limb length of top angle is increased, the buckling of more strips in compression could improve the deformation ability of the joint. Meanwhile, at the bottom angle, the length of short-limb below the bolt would also be increased which would increase the deformation ability of the joint. Nevertheless, the same failure mode prevents a large increase in load capacity of the joint.

It is worth noticing that after total vertical loads on three specimens exceeds around 60 kN, a decline on the stiffness of curves occurs, due to the overcoming of frictional force between angle limb and beam flange. The frictional force between angle and beam flange can be calculated by using the following expression:

$$V = 4\mu F \tag{4}$$

where F stands for the pre-tighten force in one bolt which is 155kN; μ for the friction coefficient which is 0.3 according to Ref. [21].

The moment resistance caused by the frictional force between angle and beam flange can be expressed as follows:

$$M_f = VH_{beam} \tag{5}$$

where H_{beam} stands for the depth of steel beam which is 0.244m.

According to the above equations, the moment resistance produced by the frictional force is calculated as 45kN.m. The experimental value referring to 60 kN of the total vertical load is 49kN.m is approximately equal to the calculated value.

From Table 3, it could be seen that different to other two specimens, the failure mode of WZ2 was pull-out of bolts only. The stiffeners of specimen WZ2 did not buckle during the loading procedure. That explains the sudden failure of joint as shown in Fig. 15(a). On the contrary, the load capacity loss of specimen WZ1 and WZ3 involved the stiffener buckling, which resulted in a slow reduction of load capacity. The buckling of stiffeners could mitigate the brittle failure of the joints. If the stiffener is too thick to buckle, the joint would suffer a sudden failure caused by the fracture of other components.

Fig. 15(b) indicates that increasing the angle thickness could not only improve the load capacity and deformation ability of the joint, but also make catenary action be triggered earlier. Meanwhile it could be seen from Fig. 15 (b-c) that increasing the length of angle short-limb has more influence on bending action than catenary action. Note that the axial force value is negative at the initial stage in Fig. 15 (b). This phenomenon was also observed in Ref. [15] and Ref. [20]. This may be due to the fact that the rotation center of joint is higher than the rotation center of pin supports. After the vertical load is applied, “arch action” is developed by treating the rotation center of joint and pin supports as arch crown and arch spring respectively. However, more test results are still needed for fully understanding this phenomenon. Fig. 15(d) shows the comparison of moment-axial force relationship of three specimens. It can be seen that the curve representing specimen WZ3 shows the similar trend to the proposed theoretical curve in Ref. [18] and Ref. [27]. However, the moment-axial force relationship of specimen WZ1 and WZ2 shows a different pattern that the moment of joint does not decrease with the increase of axial force. It may be due to the early formation of catenary action. This phenomenon implies that the configuration of joint directly affects the moment-axial force relationship pattern of joints which is not consistent in practice. More studies should be conducted on the patterns of moment-axial force relationship of joint in the future.

The comparison between the load capacity of specimen with and without considering catenary action is shown in Table 4. Generally, catenary action could enhance the anti-collapse behavior of three joints. For specimen WZ1, catenary action could increase its the load capacity and deformation ability. The enhancement of catenary action for specimen WZ2 and WZ3 is noteworthy. The load capacity of specimen WZ2 is increased by 45 percent due to catenary action, whilst its deformation ability is only increased by 16 percent which is even less than that of specimen WZ1. Meanwhile, if only bending action is considered, specimen WZ3 could almost achieve its load capacity. On the contrary, the deformation ability of specimen WZ3 is significantly enhanced by 92 percent.

3.6. Practical implications of the experimental results

The configurations of steel joints recommended by Department of Defense (DoD) [2] are divided into three categories, namely fully restrained moment connections (FRMC), partially restrained moment connections (PRMC), partially restrained connections (flexible). Bolted joint using stiffened angle developed in this study is not covered by DoD. Due to the capacity enhancement by the extra stiffeners used at the angles, the proposed joint may be categorized as FRMC or PRMC, based on the bending behavior and configuration details of the connection. Therefore, the acceptance in DoD still could be used to assess the proposed connection.

Fig.17 shows the rotation capacity comparison between experimental results and the acceptance criteria of DoD for FRMC and PRMC. Experimental results with considering catenary action show much higher rotation capacities than the acceptance criteria for FRMC and PRMC in DoD. Except for specimen WZ2, experimental results without considering catenary action match well with the acceptance for FRMC in DoD, but still show much higher rotation capacities than the acceptance for PRMC. Thus, these acceptances criteria in DoD may be too conservative for this type of joint in this study. Similar conclusions were also drawn by Ref. [14-15]. It may be explained by the fact that these acceptance criteria for nonlinear analysis of steel frame connections in DoD [2] are determined primarily from the seismic tests, without considering catenary action. Meanwhile, CFST columns could provide stronger restraint for the connections under loads, compared with bare steel columns. It indicates that new nonlinear acceptance criteria for connection rotation capacity should be proposed with considering the contribution of catenary action.

3.7. Component method in joint performance assessment

Component method is recommended in EC 3 [23] to predict the performance of steel connection. The structural components for the joint with stiffened angle and long bolts under flexural action in this study involve: bolts in tension (bt), bolts in shear (bs), bolts in bearing (bb), stiffened angle in tension (sat) and column in compression (cc), as shown in Table 5. It should be mentioned that the component of stiffened angle in tension is not covered in Eurocode 3. In this study, the stiffened angle is modeled by a T-stub, due to the strengthen effect of stiffener to the angle.

Table 6 shows the component model of stiffened angle joint with long bolts. The components 1 to 4 in Table 5 are basic components whose design methods for stiffness coefficient are provided in detail in Eurocode 3. It is worth noticing that bolt pretension effect which plays an important role in rotation stiffness of joint is not considered in Eurocode 3. The stiffness coefficient k_{bt} of bolts in tension is obtained by Eq. (6) in Eurocode 3:

$$k_{bt} = 2c_p A_b / L_b \qquad (6)$$

where A_b is the effective area of bolt; L_b is the bolt elongation length which is equal to the grip length, plusing half the sum of the height of the bolt head and nut. The coefficient c_p is 0.8 if considering the effect of prying force and 1.0 if prying force is not triggered or taken into account, respectively.

In fact, if bolt pretension is ignored in this test, the coefficient k_{bt} for bolts in tension would be very small, since long bolts are used in the joints which would cause a large value of bolt elongation length L_b. Based on the expression in Ref. [24], Eq. (7) is proposed to determine the stiffness coefficient of preloaded long bolts used in this study:

$$k_{bt} = 2c_p(5.25 + 3.25\frac{B_c + 2t_{sa}}{d_b})\frac{A_b}{L_b} \qquad (7)$$

where B_c stands for the width of column; t_{sa} for the thickness of angle; d_b for the diameter of long bolt.

Due to the preloads in bolts, the stiffness coefficient of component 2 and component 3 could be taken as equal to infinity [23]. Thanks to the existence of in-filled core concrete and symmetry of loading condition, the stiffness and capacity of component 5 could also be taken as equal to infinity [10]. If hollow section column is used, the stiffness and capacity of component 5 should be considered in component method. It should be mentioned that, with the increase of connection deformation, column in compression would cease to act any longer and the stiffened angle above the beam flange would be activated as a component in tension.

Based on the component model in Table 6, the initial stiffness S_{ini} of joints could be determined from Eq. (8) in Eurocode 3 [23]:

$$S_{ini} = \frac{E_s z_{eq}^2}{1/k_{eq}} \qquad (8)$$

where E_s stands for Young's modulus of steel; z_{eq} for the equivalent lever arm; k_{eq} for the equivalent coefficient.

As shown in Table 6, good agreements are obtained between the model considering pretension effect and test results. On the contrary, a large discrepancy shows up without considering pretension effect. It is worth to notice that the experimental initial stiffness of WZ3 is close to that of WZ2 in the test whilst the computational result of WZ3 is identical to that of WZ1. As shown in Table 6, the computational initial stiffness of the joint depends on the stiffness coefficient and lever arm which are identical in WZ1 and WZ3. Increasing the length of short limb makes no difference to the component model. In practice, increasing the length of short limb would increase the initial stiffness of the joint, which is due to the fact that longer short limb and stiffener would make a better transfer of internal force to the T-stub in row 5. However, the model of T-stub can not present the influence of the length of

short limb and stiffener. More studies would be carried out in the future to propose a precise model for stiffened angle in tension.

4. Numerical analysis

4.1. Finite element modeling

Based on the test, a finite element model is developed by ABAQUS. Solid elements (C3D8R) are used to simulate the components of the joint. Due to the symmetry of specimens and loading condition, only half of the joint is modeled as shown in Fig. 18. The normal and tangential behavior of the interaction between members (such as, steel tube and concrete, bolts and steel plate) are defined as "hard contact" and "penalty" with a friction coefficient respectively in ABAQUS. The values of 0.3 [25] and 0.35 [21] are assigned to the friction coefficient for steel tube to core concrete and bolt to steel plate respectively. The welding between fin plate and column wall is not modeled, since no fracture was observed between them in all three tests. In that case, fin plate is merged with column wall in the model. The boundary condition of the model is identical with that of the testing specimen. The command of *Bolt Load in ABAQUS is adopted to simulate the pre-tension loads in high-strength bolts.

Elastic-plastic material model and the Concrete Plastic Damage (CPD) material model in ABAQUS are employed to simulate steel and concrete members respectively. The parameters for CPD model are listed in Table 7. The material properties of concrete and steel members are taken as those in the material test. The stress-strain relationship of steel is shown in Fig. 19 while that of concrete in compression is determined by Eq. (9) [26]:

$$\begin{cases} y = 1.9x - 0.8x^2 - 0.1x^3 & (x \le 1) \\ y = x / (1.94(x-1)^2 + x) & (x > 1) \end{cases} \quad (9)$$

where $x=\varepsilon/1790$; $y=\sigma/40$.

In order to simplify the analysis, a linear stress-strain relationship is used for concrete in tension. 10% and 1% of the compressive strength of concrete is considered as the tensile strength and remaining strength of concrete after cracking in tension.

Strain-based fracture criterion in ABAQUS is adopted to predict the failure mode of the specimen. The fracture strain of 0.28 as tested is used for stiffened angels. Static solver is adopted to conducte the analysis, since the explict dynamic solver is computational expensive. In that case, the fracture evolution would not be simulated by static solver, but only peak load is attained when the solver ceases to run due to excessive cracking.

4.2. Model validation

As shown in Fig. 20, the finite element model is validated against the test results whilst an extra test data collected from Ref. [18] is also adopted. A good agreement is achieved between the simulation and experimental results, in term of load capacity, initial stiffness and deformation performance as listed in Table 8. Fig. 21 shows the deformation of specimen WZ1 and the finite element model. The experimental phenomena such as stiffener buckling and angel deformation are successfully represented in finite element (FE) model. The comparison between load-displacement curves and deformation phenomena both illustrate the reliability and effectiveness of the FE models.

4.3. Influence of bolt arrangement

According to the experimental results, increasing the length of short-limb is not an effective method to improve the behavior of the joint, comparing to increasing limb thickness. However, an extra row of bolts could be arranged at the enlongated short-limb. In that case, a new model WZL is designed as shown in Fig. 22.

Fig. 23 shows the influence of bolt arrangement. Compared to FE model of WZ3, extra row of bolts has little effect on the performance of the joints in early stage. With the vertical displacement increasing, after tensile failure of bottom row of bolts in WZL which results in the sudden drop in the vertical force-displacement curve, the extra row of bolts began to resist load. Ultimately, the load capacity and deformation ability of WZL are both better than those of WZ3. It may also be concluded that extra row of bolts could enhances the redundancy of the joint. Once the bottom row of bolts fails, extra row of bolts could provide alternative transmission path for internal force on the joint. Also, catenary action would be triggered earlier by setting extra row of bolts as shown in Fig. 23(b).

5. Equivalent dynamic response evaluation

It is known that, the response of structures after column removal are normally dynamic. However, dynamic experiments and analysis are complex and high consumption of resources. To solve these problems, a simplified method to calculate equivalent dynamic response of structures was developed by Izzuddin et al. [27], which can be expressed by Eq. (10):

$$P_{0,n} = \frac{1}{u_{d,n}} \int_0^{u_{d,n}} P du_s \qquad (10)$$

where P stands for the static load; u_s for the static diplacement; $P_{0,n}$ for the level of suddenly load; $u_{d,n}$ for the maximumn dynamic diplacement .

As shown in Fig. 24, the maximum equivalent dynamic response can be determined from the equivalence between internal energy and external work, according to a nonlinear static analysis curve.

The static response (P, u_s) curve and the equivalent dynamic response ($P_{0,n}$, $u_{d,n}$) curve of three specimens based on the simplified method are shown in Fig. 25 (a, c, e). The unloading portions of the experimental curves are not presented. From the comparison of static response and equivalent dynamic response, it can be seen that the dynamic vertical displacement is larger than the static vertical displacement at any load level. The dynamic amplification coefficient (DAC) is defined as the ratio of static load to dynamic load.

The applicability of dynamic amplification coefficient in DoD has been assessed by some researches [28-29]. It shows that the difference between the DoD provision and the experimental study varies remarkably with the different configuration of connection. Fig. 25 (b, d, f) show the DAC derived from the simplified method and the values recommended by DoD [2]. When the vertical displacement is small, the DAC from the simplified method is around 2.0 which is close to the value recommended by DoD. Along with the increase of vertical displacement, even the trend of two curves is similar, the difference between two curves is increasing, especially for specimen WZ2. It could be seen from Fig. 25(d) that the DAC of specimen WZ2 remains almost unchanged after catenary action begins to carry load. Compared with the results in Fig. 15, the displacement corresponding to the mobilization of catenary action is the same as the displacement corresponding to the cease of DAC decreasing. It could be explained that catenary action which plays a key role in load-bearing capacity of the joints at large vertical displacement stage has significant effect on the DAC, whilst catenary action may not be considered in DoD provision.

6. Conclusions

A steel-beam to CFST-column connection with stiffened angle and fin plate joints was developed. Three specimens were designed and tested in the scenario of middle column loss. The failure modes and development of catenary action are discussed in detail. The following conclusions are made as follows:

1. The performance of the proposed joint could be improved significantly by increasing the angle thickness. Increase of the length of angle short-limb has influence on the deformation ability of the proposed joint, rather than the load capacity. Increasing the angle thickness could bring an early formation of catenary action whilst increasing the length of angle short-limb has more influence on bending action than catenary action.

2. The stiffener buckling could slow down the decline of load capacity at the final stage of loading. In other words, the buckling of stiffeners could prevent the brittle failure of the joints.

3. With the contribution of catenary action, the joints show much higher rotation capacities than the acceptance criteria stipulated by DoD. Current acceptance criteria of connection rotation capacities can be advisedly improved to consider the contribution of catenary action.

4. Component method is used to calculate the initial stiffness of the joints. With considering the pretension effect in bolts, the computational results match well with the test results. New component needs to be developed to present the stiffened angle in tension in design codes.

5. Based on numerical results, adding extra row of bolts could improve the load capacity and deformation ability of the proposed joint. Also, catenary action would be triggered earlier by extra row of bolts.

6. When the vertical displacement is small, the dynamic amplification coefficient (DAC) derived from the simplified method is close to the values recommended by DoD. The difference between them is increasing with the increase of vertical displacement. It shows that dynamic amplification coefficient should be worked out considering catenary action under large deformation.

Acknowledgements

The project is supported by National Natural Science Foundation of China (No. 51408106), China Postdoctoral Science Foundation (No. 2017M622965), Key projects of key R & D projects in the Ningxia Hui Autonomous Region (2018BEG02009), Shaanxi Key Laboratory of safety and durability of concrete structures (XJKFJJ201803) and Xijing University Special Foundation (XJ17T07) which are gratefully acknowledged.

References

[1] United States General Services Administration (GSA). Progressive collapse analysis and design guidelines for new federal office buildings and major modernization projects. Washington (DC). 2003.

[2] U.S. Department of Defense. Unified Facilities Criteria: Design of Building to Resist Progressive Collapse. UFC 4-023-03, USA, 2013.

[3] Cerfontaine F., Jaspart J.-P. Analytical study of the interaction between bending and axial force in bolted joints. Steel Structures-Eurosteel 2002, Cmm Press, Coimbra 2002:997-1006.

[4] Simoes da Silva L., Lima L.R.O., Vellasco P.C.G., Andrade S.A.L. Behaviour of flush end-plate beam-to-column joints under bending and axial force. Steel Composite Structure. 2004, 4(2):77-94.

[5] Del Savio A.A., Nethercot D.A., Vellasco P.C.G., Andrade S.A.L. Martha L.F. Generalized component-based model for beam-to-column connections including axial versus moment interaction. Journal of Constructional Steel Research. 2009, 65:1876-1895.

[6] Hoang V.L., Jaspart J.P., Demonceau J.F. Extended end-plate to concrete-filled rectangular column joint using long bolts. J. Constr. Steel Res., 2015, 113: 156-168.

[7] Kloiber L. Designing HSS connections. Modern Steel Construction, November, 2001.

[8] McCormick J. Connecting hollow structural section members with through-bolts. Steel Tube Institute, June, 2017.

[9] Wang J.F., Chen L.P. Experimental investigation of extended end plate joints to concrete-filled steel tubular columns. J. Constr. Steel Res., 2012, 79: 56-70.

[10] Thai H.T., Uy B. Rotational stiffness and moment resistance of bolted endplate joints with hollow or CFST columns. J. Constr. Steel Res., 2016, 126: 139-152.

[11] Huang W.J., Fenu L., Chen B.C. Experimental study on joint resistance and failure modes of concrete filled steel tubular (CFST) truss girders. J. Constr. Steel Res., 2018, 141: 241-250.

[12] Khandelwal K. and EI-Tawil S. Collapse behavior of steel special moment resisting frame connections, Journal of Structural Engineering, 2007, 133(5), 646-655.

[13] Demonceau J.F., Jaspart J.P. Experimental and analytical investigations on the behavior of building frames further to a column loss, Conference: ASCE Structures Congress 2009, USA, Austin.

[14] Sadek F., Main J.A., Lew H.S. and Bao Y.H. Testing and analysis of steel and concrete beam-column assemblies under a column removal scenario, Journal of Structural Engineering, 2011, 9: 881-892.

[15] Yang B., Tan K.H. Experimental tests of different types of bolted steel beam–column joints under a central-column-removal scenario, Engineering Structures, 2013, 54: 112-130.

[16] Li L., Wang W., Chen Y.Y. and Lu Y. Experimental investigation of beam-to-tubular column moment connections under column removal scenario, Journal of Constructional Steel Research, 2013, 88(5), 244-255.

[17] Stylianidis P.M. and Nethercot D.A. Modelling of connection behaviour for progressive collapse analysis, Journal of Constructional Steel Research, 2015, 113:169-184.

[18] Gao S., Guo L.H., Fu F., Zhang S.M. Capacity of semi-rigid composite joints in accommodating column loss. Journal of Constructional Steel Research, 2017, 113:169-184.

[19] Daneshvar H, Driver R G. Behaviour of shear tab connections in column removal scenario. Journal of Constructional Steel Research, 2017, 138: 580-593.

[20] Gong Y. Test, modeling and design of bolted-angle connections subjected to column removal. Journal of Constructional Steel Research, 2017, 139: 315-326.

[21] GB50017-2017. Code for design of steel structures. Beijing, China, 2017.

[22] GB50936-2014. Technical code for concrete filled steel tubular structures. Beijing, China, 2014.

[23] European committee for standardization. Eurocode 3: design of steel structures—Part 1-1: general rules and rules for buildings, BS EN 1993-1-1:2005. British Standards Institution, UK; 2005.

[24] Faella C., Piluso V., Rizzano G. Experimental analysis of bolted connections: snug versus preloaded bolts. Journal of Structural Engineering, 1998, 124: 764-744.

[25] Peter B., Atle G. Coefficient of friction for steel on concrete at high normal stress. Journal of Material in Civil Engineering. 1990, 2(1): 46-49.

[26] GB50010-2010. Code for design of concrete structures. Beijing, China, 2015.

[27] Izzuddin B.A., Vlassis A.G., Elghazouli A.Y., Nethercot D.A. Progressive collapse of multi-storey buildings due to sudden column loss-Part 1: Simplified assessment framework. Engineering Structures, 2008,30(5): 1308-1318.

[28] Fu Q.N., Yang B., Hu Y. et al. Dynamic analyses of bolted-angle steel joints against progressive collapse based on component-based model. Journal of Constructional Steel Research, 2016, 117: 161-174.

[29] Li H.H., Cai X.H., Zhang L. et al. Progressive collapse of steel moment-resisting frame subjected to loss of interior column: Experimental tests. Engineering Structures, 2017, 150: 203-220.

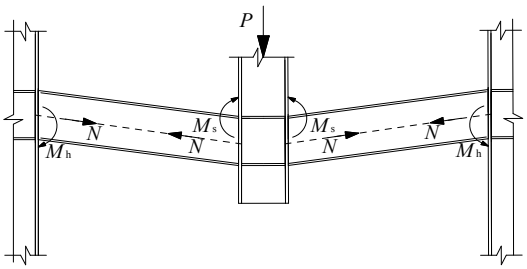

Fig. 1 Load-carrying action transition

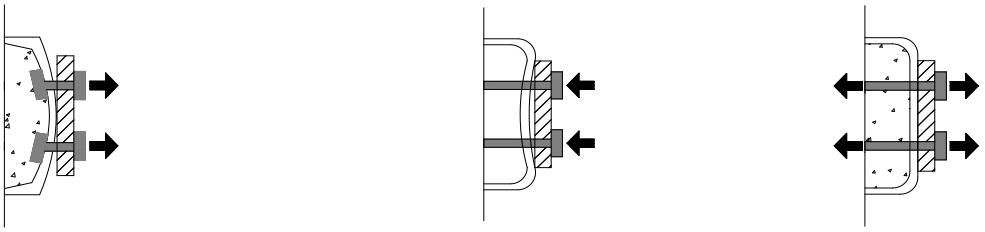

(a) Blind bolt in CFST or hollow section column (b) Long bolt in hollow section column (c) Long bolt in CFST column

Fig. 2 CFST column and hollow section column bolted joints

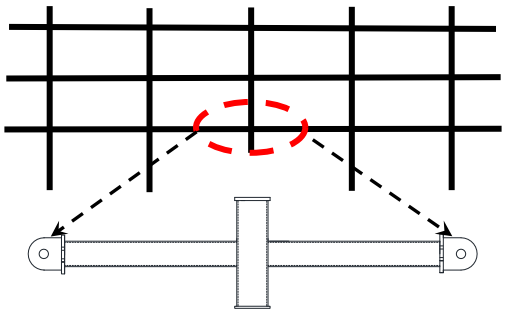

Fig. 3 Sub-structure specimen

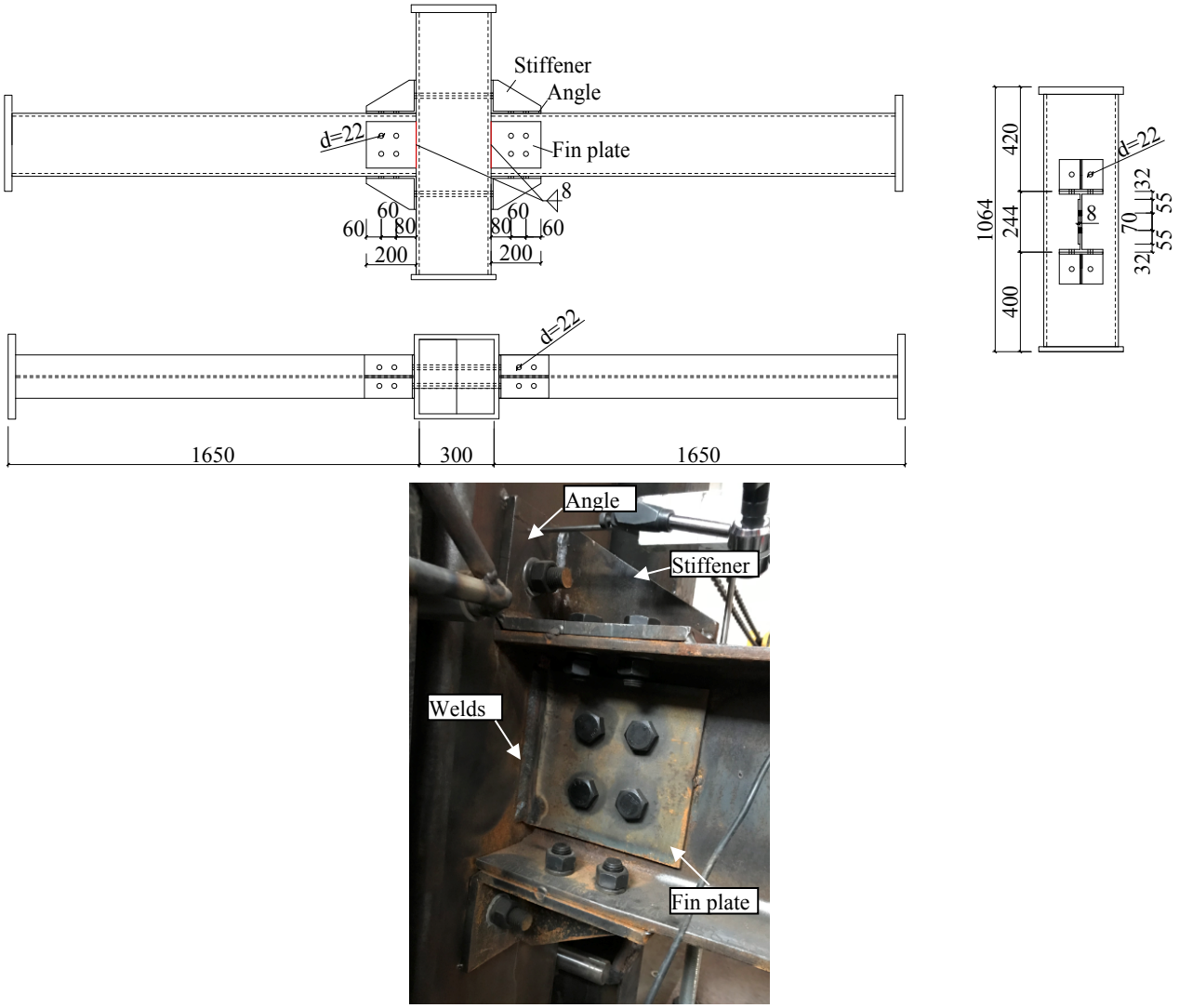

(a) Configuration of specimens

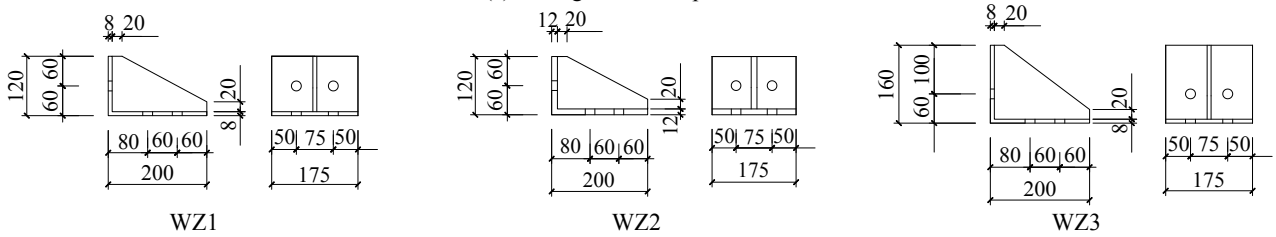

(b) Details of angles

Fig. 4 Dimensions of specimens (all dimensions are in mm)

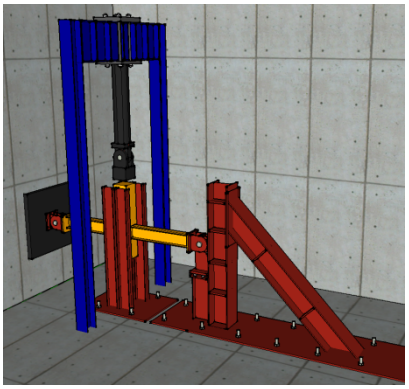

(a) Aerial view

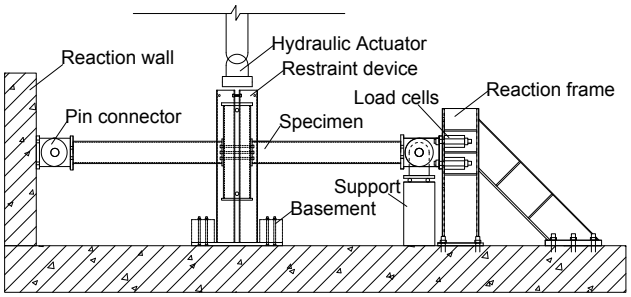

(b) Elevation view

(c) Out-plane restraint device

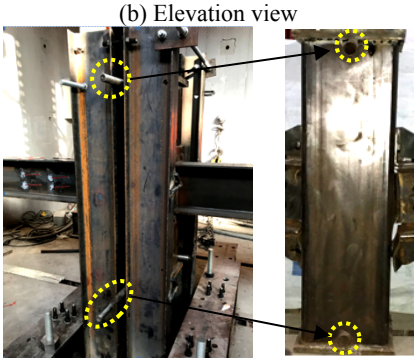

(d) In-plane restraint device

Fig. 5 Test rigs

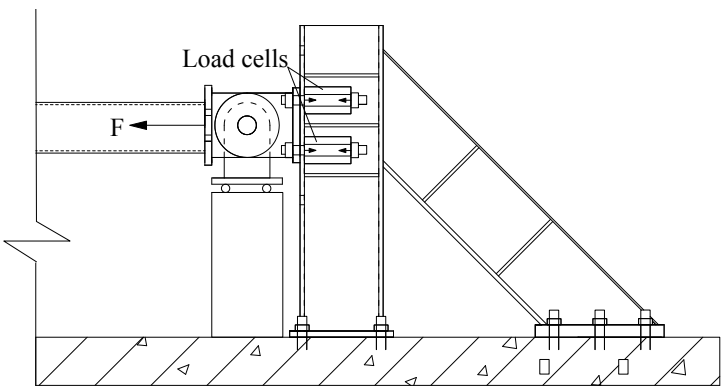

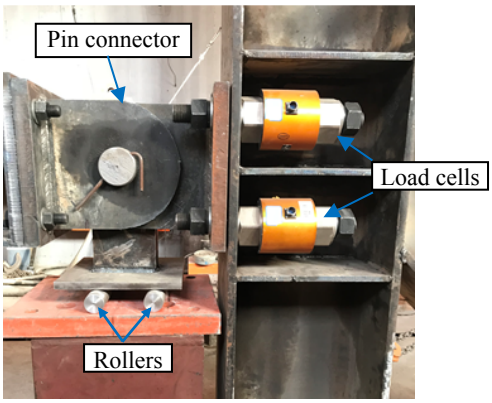

Fig. 6 Horizontal load cells

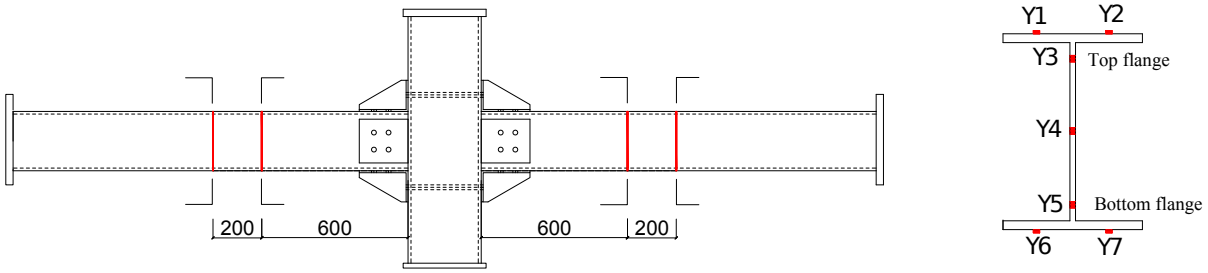

(a) Strain gauges

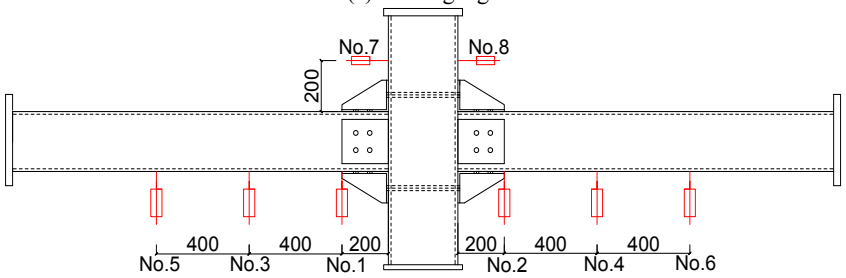

(b) LVDTs

Fig. 7 Distribution of measuring equipments

(a) Deformation of the short-limb of bottom angle

(b) Buckling of stiffener at top angle

(c) Pull-out of bolts

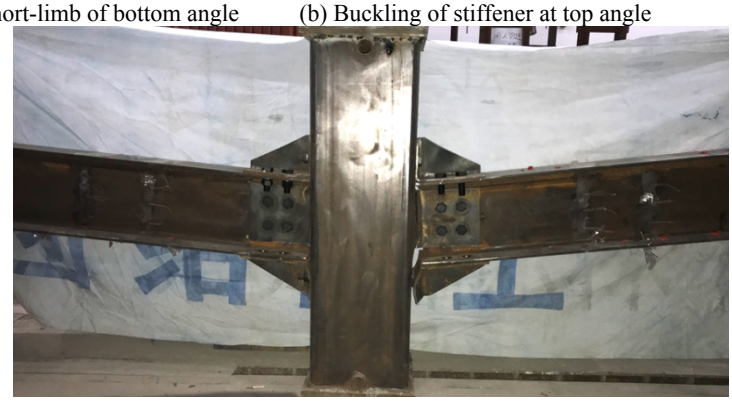

(d) Failed specimen

Fig. 8 Phenomenon of WZ1

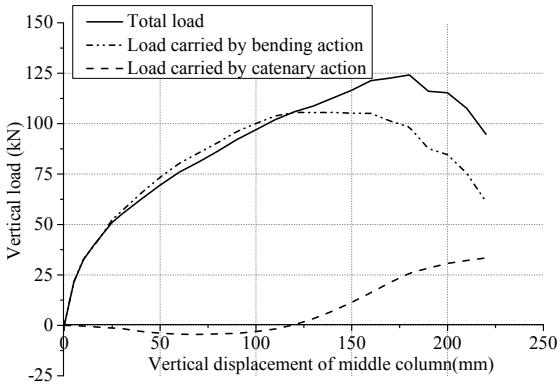

(a) Vertical force–middle column displacement curve

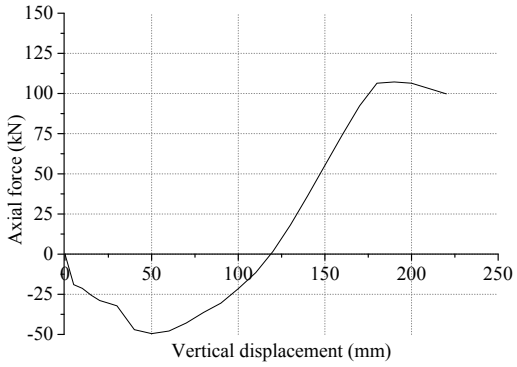

(b) Axial force of left beam-vertical displacement curve

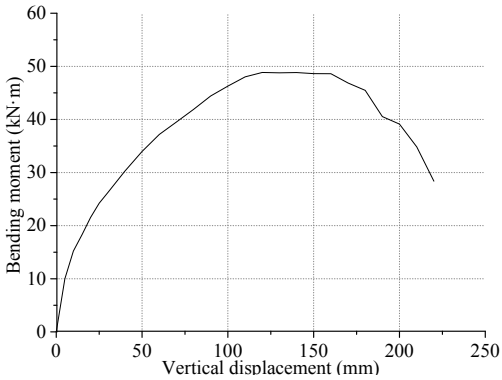

(c) Bending moment of left connection-vertical displacement curve

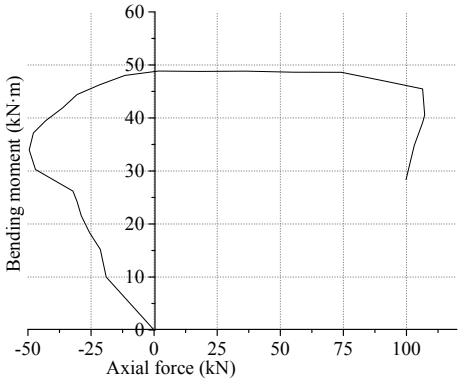

(d) Moment-axial force relationship curve

Fig. 9 Experimental results of WZ1

(a) Deformation of the short-limb bottom angle

(b) Gap between beam flange and long-limb

(c) Pull-out of bolts

(d) Failed specimen

Fig. 10 Phenomenon of WZ2

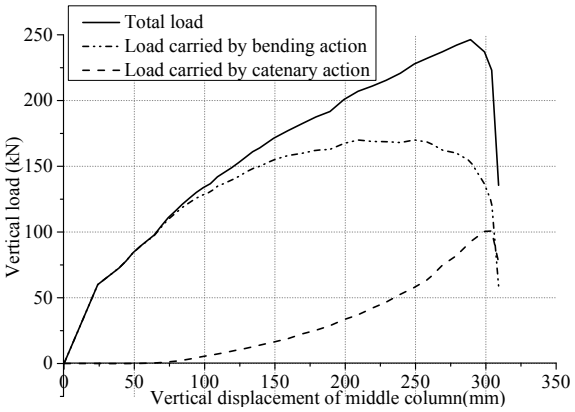

(a) Vertical force–middle column displacement curve

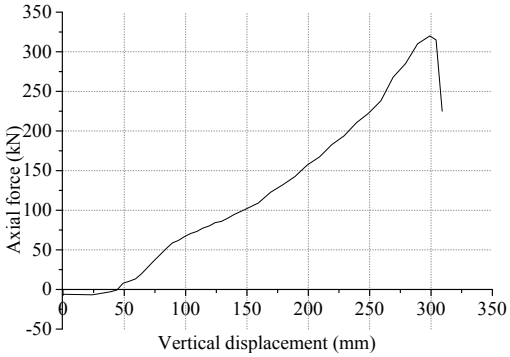

(b) Axial force of left beam-vertical displacement curve

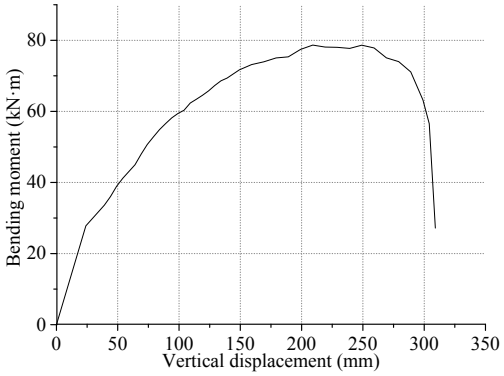

(c) Bending moment of left connection-vertical displacement curve

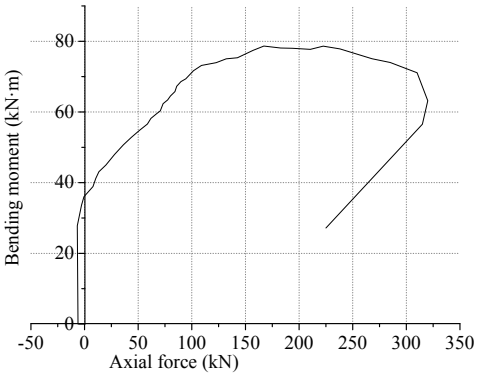

(d) Moment-axial force relationship curve

Fig. 11 Experimental results of WZ2

(a) Gap between beam flange and column flange

(b) Buckling of stiffener at top angle

(c) Pull-out of bolts

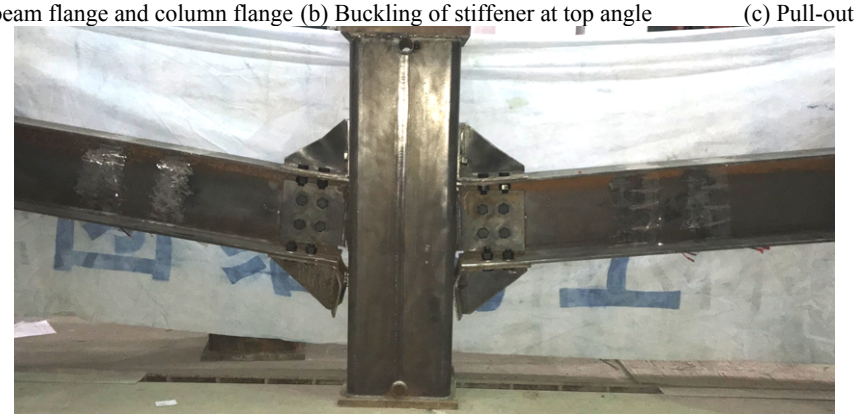

(d) Failed specimen

Fig. 12 Phenomenon of WZ3

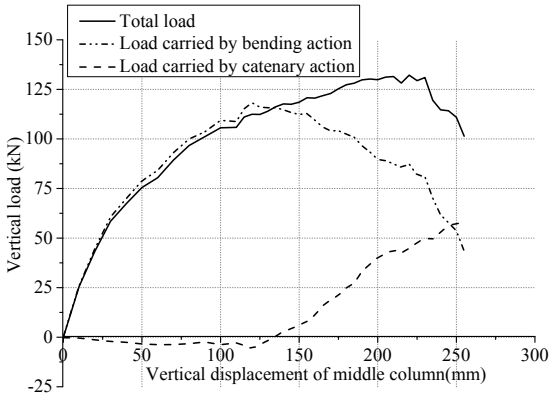

(a) Vertical force–middle column displacement curve

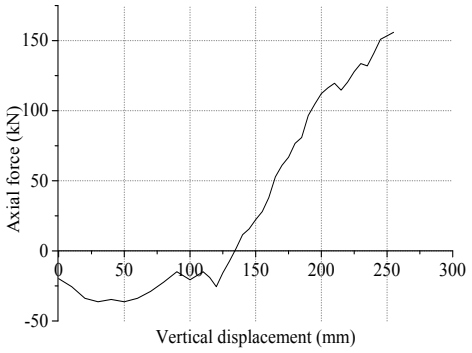

(b) Axial force of left beam-vertical displacement curve

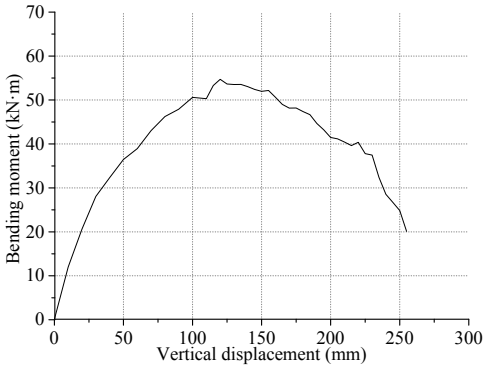

(c) Bending moment of left connection-vertical displacement curve

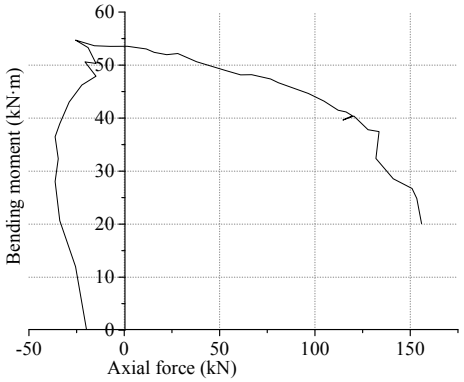

(d) Moment-axial force relationship curve

Fig. 13 Experimental results of WZ3

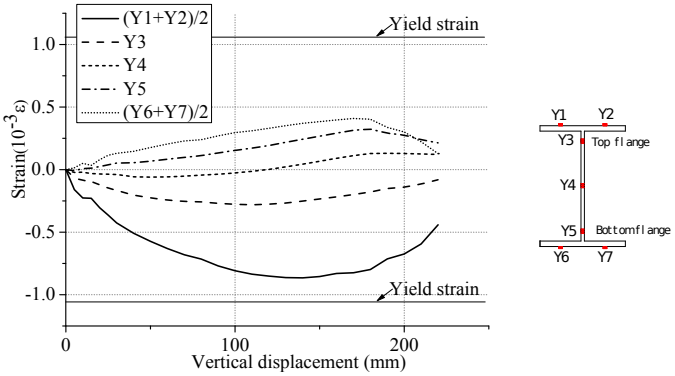

(a) Strain distribution on steel beam

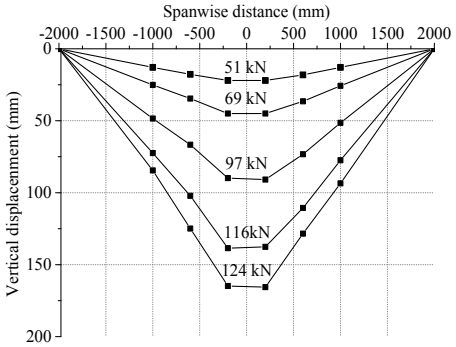

(b) Beam displacement profiles corresponding to indicated vertical loads

Fig. 14 Strain and deformation data of specimen WZ1

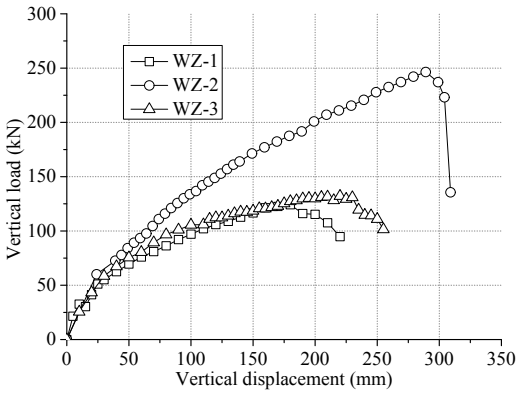

(a) Vertical force–middle column displacement curve

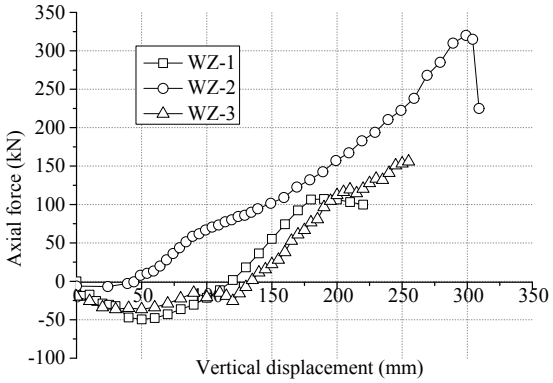

(b) Axial force of left beam-vertical displacement curve

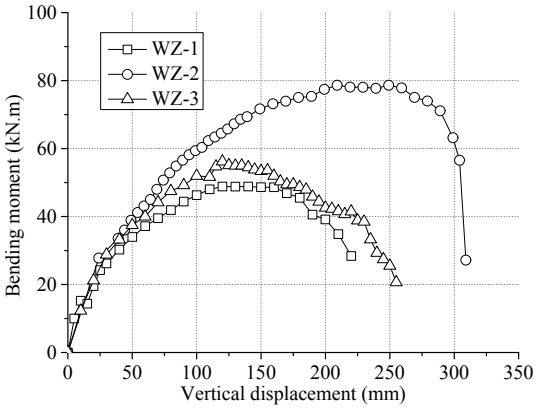

(c) Bending moment of left connection-vertical displacement curve

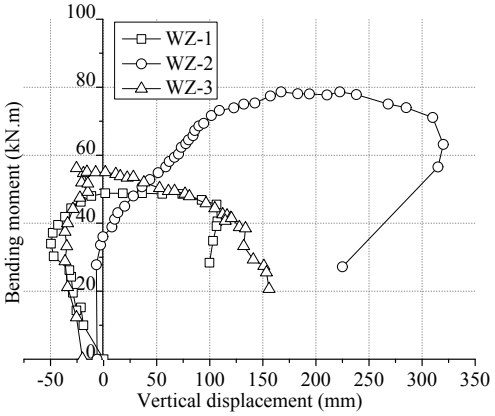

(d) Moment-axial force relationship curve

Fig. 15 Comparison of the behavior of three specimens

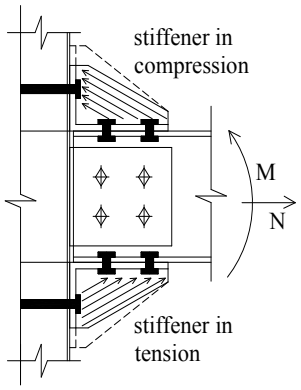

Fig. 16 Mechanical model of stiffeners

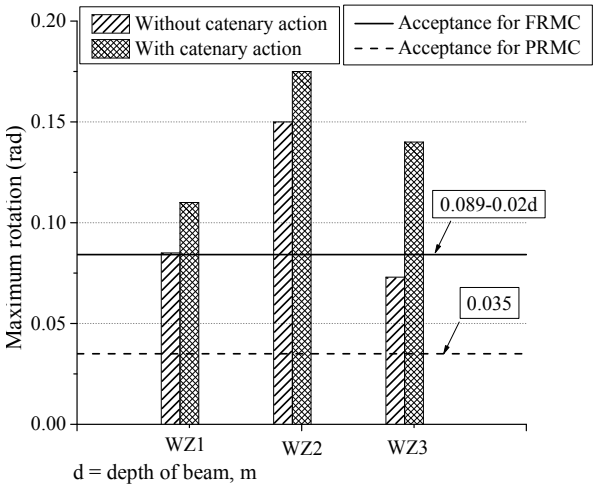

Fig. 17 Comparison of joint rotation capacities between the experimental results and DoD [2]

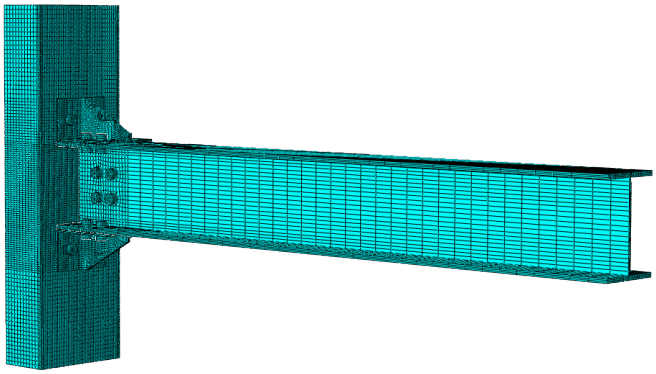

Fig. 18 Finite element model

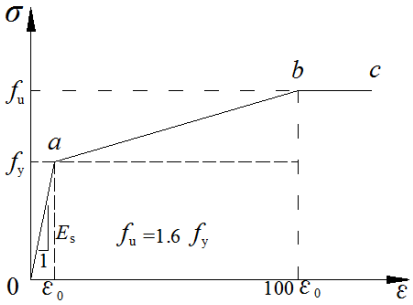

Fig. 19 Stress-strain relationship of steel

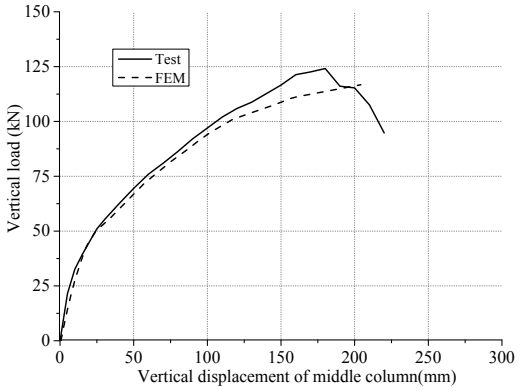

(a) WZ1

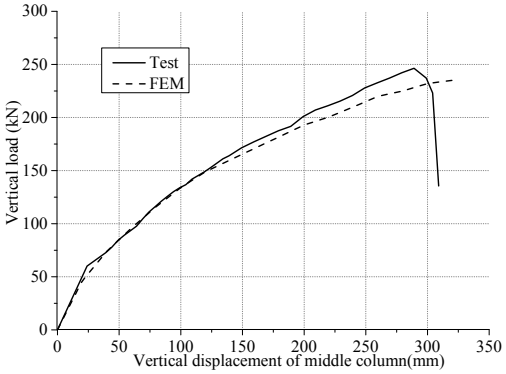

(b) WZ2

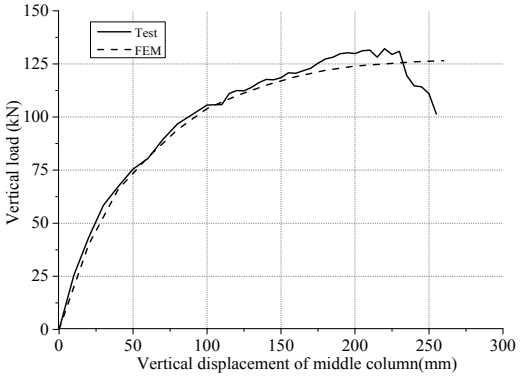

(c) WZ3

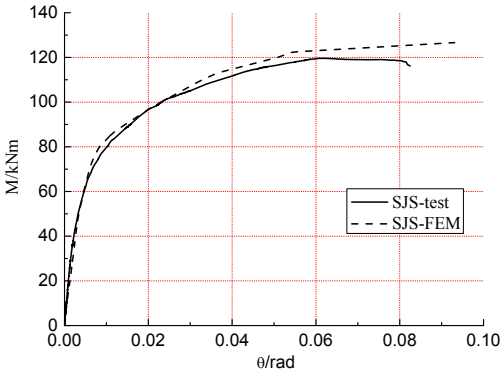

(c) Specimen in Ref. [18]

Fig. 20 Validation of finite element model (Vertical load-displacement curves)

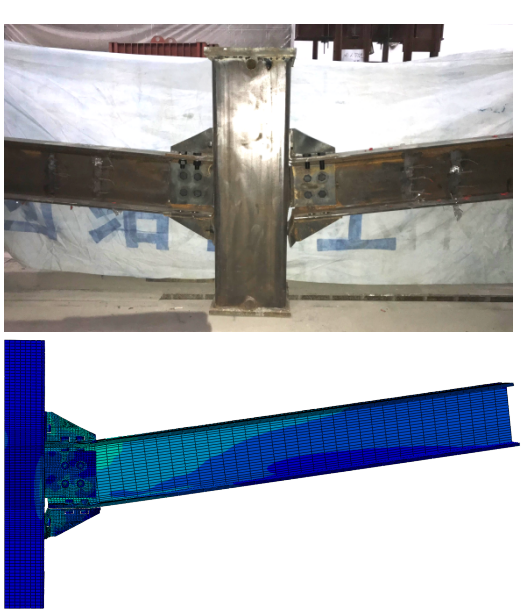

(a) Deformation at maximum displacement

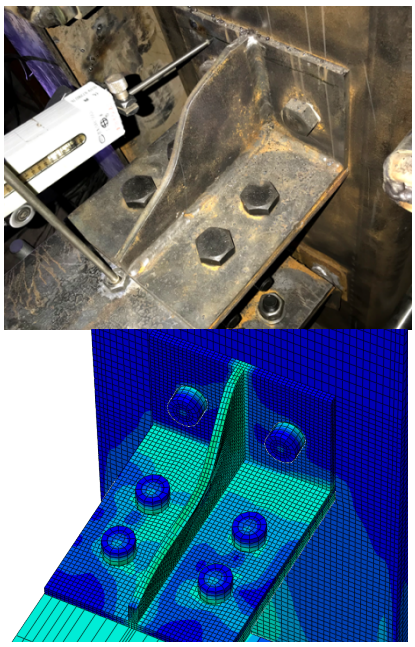

(b) Stiffener buckling

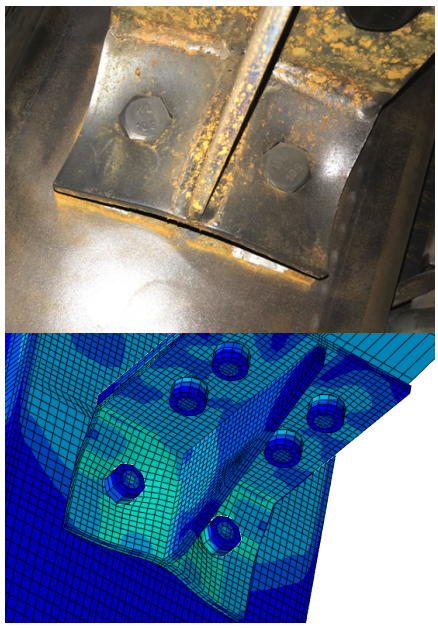

(c) Deformation of angle short-limb

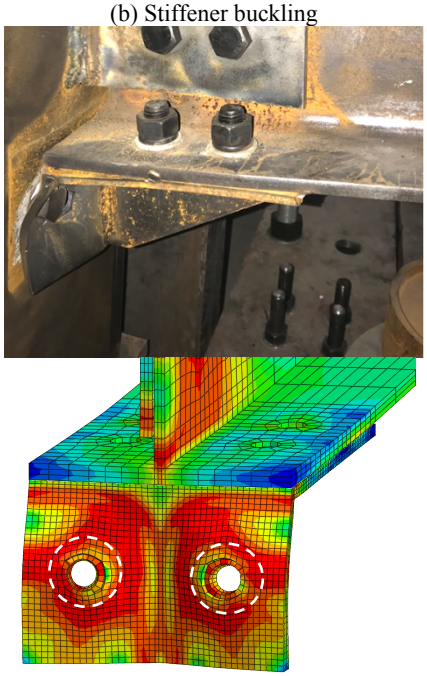

(d) Failure of bolt hole

Fig. 21 Validation of finite element model (Experimental phenomena of specimen WZ1)

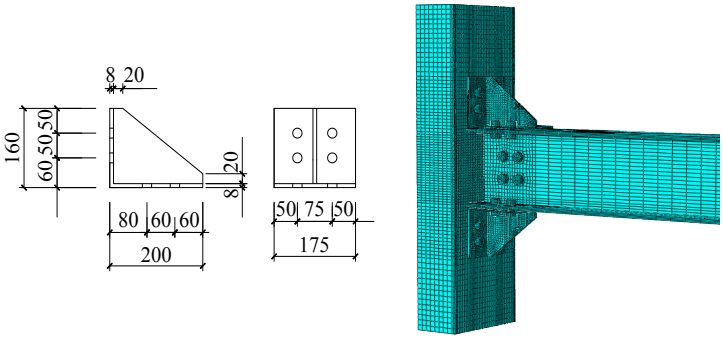

(a) Dimensions of the elongated angle (b) Finite element model

Fig. 22 FE model of WZL with extra row of bolts

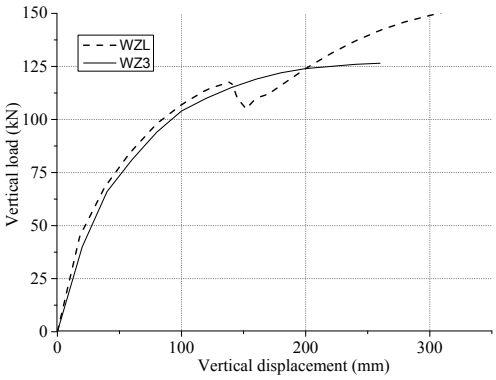

(a) Vertical force–displacement curve

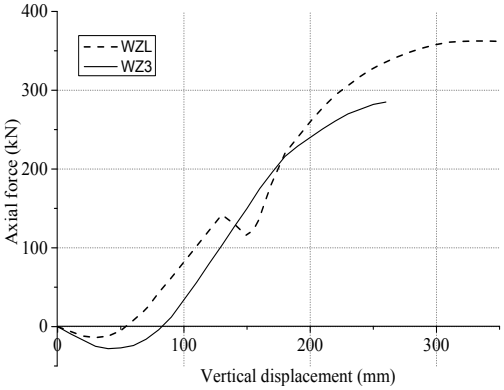

(b) Axial force of left beam-vertical displacement curve

Fig. 23 Influence of bolt arrangement

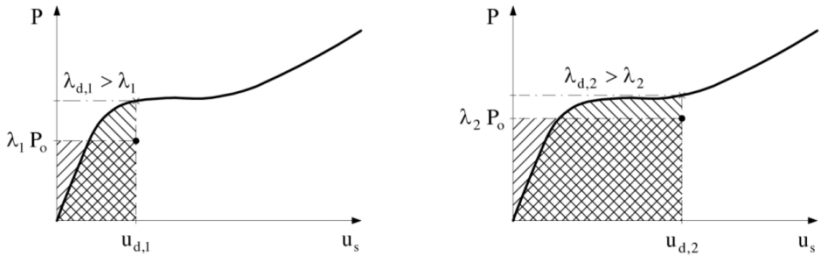

(a) Dynamic response ($P = \lambda_1 P_o$) (b) Dynamic response ($P = \lambda_2 P_o$)

Fig. 24 Equivalent dynamic response evaluation [26]

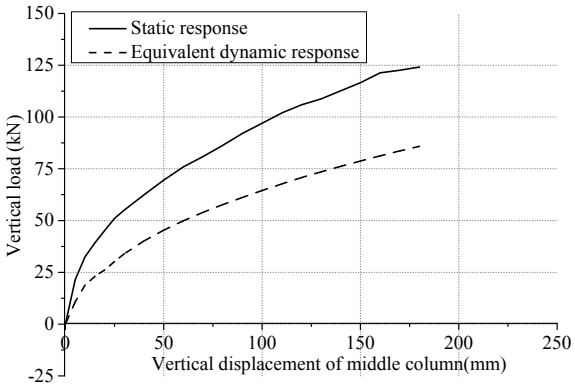

(a) Comparison of static response and dynamic response(WZ1)

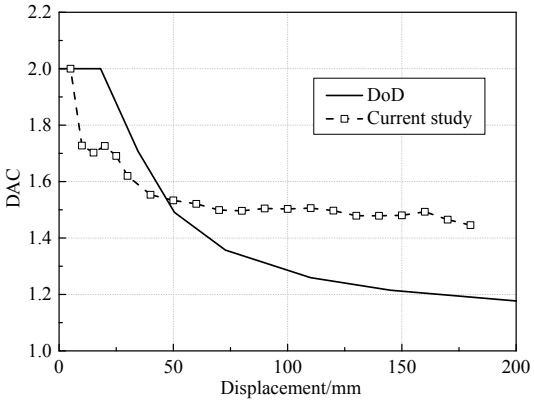

(b) Dynamic amplification coefficient (WZ1)

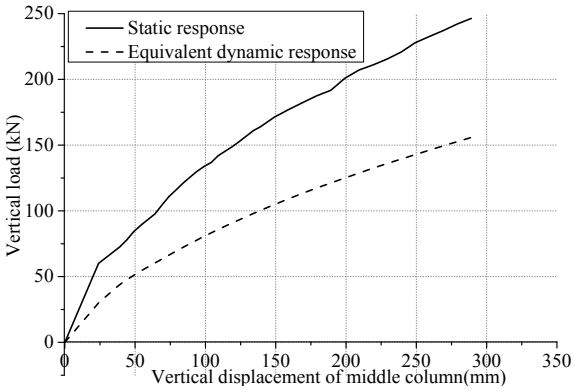

(c) Comparison of static response and dynamic response(WZ2)

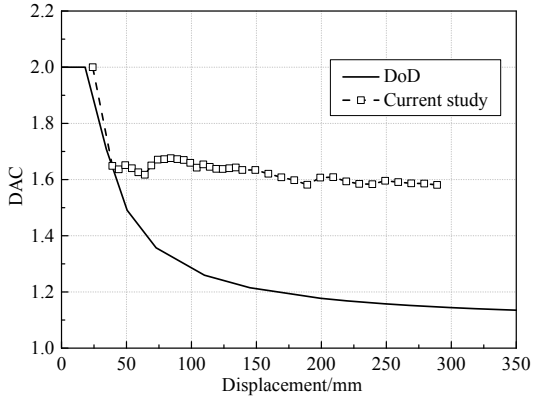

(d) Dynamic amplification coefficient (WZ2)

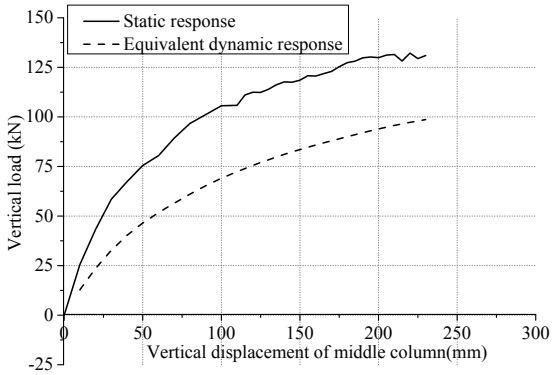

(e) Comparison of static response and dynamic response(WZ3)

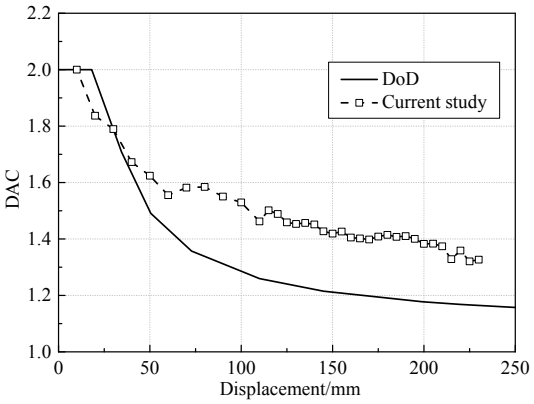

(f) Dynamic amplification coefficient (WZ3)

Fig. 25 Equivalent dynamic response evaluation

Table 1 Parameters of specimens

Specimen ID	Steel members			Bolt diameter/mm	Pretension/kN
	Column	Beam	Angle		
WZ1	□300×300×12	HM244×175×7×11	∟200×120×8	20	155
WZ2	□300×300×12	HM244×175×7×11	∟200×120×12	20	155
WZ3	□300×300×12	HM244×175×7×11	∟200×160×8	20	155

Table 2 Mechanical properties of steel

Se.		f_y（MPa）	f_u（MPa）	E_s（10^5MPa）	ε_u
Beam	Flange	218	454	2.04	0.23
	Web	321	467	2.03	0.31
Angle	L1/L3	374	499	2.01	0.34
	L2	348	460	2.03	0.32
Tube wall		381	490	2.05	0.34
Bolt		1089	1210	2.06	-

Table 3 Experimental results of three specimens

Specimen ID	Maximum vertical load /kN	Maximum vertical displacement/mm	Maximum bending moment /kN • m	Maximum axial force /kN	Failure mode
WZ-1	124.2	180.0	48.8	107.2	Bolts pull-out and stiffener buckling
WZ-2	246.3	289.0	78.6	320.4	Bolts pull-out
WZ-3	130.9	230.0	41.5	155.9	Bolts pull-out and stiffener buckling

Table 4 Comparison of joint performance with and without catenary action

Specimen ID	Load capacity with catenary action/kN	Deformation ability with catenary action/mm	Load capacity without catenary action /kN	Deformation ability without catenary action/mm	Load capacity increase due to catenary action /%	Deformation ability increase due to catenary action /%
WZ-1	124.2	180.0	105.6	140.0	18	28
WZ-2	246.4	289.0	170.0	250.0	45	16
WZ-3	130.9	230.0	118.3	120.0	11	92

Table 5 Component identification

1. Bolts in tension	2. Bolts in shear	3. Bolts in bearing	4. Stiffened angle in tension	5. Column in compression (under flexural action)
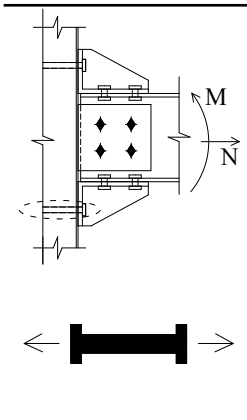	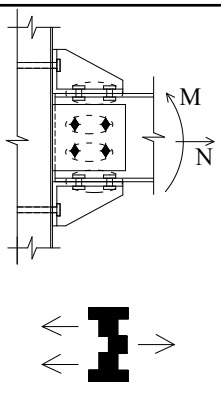	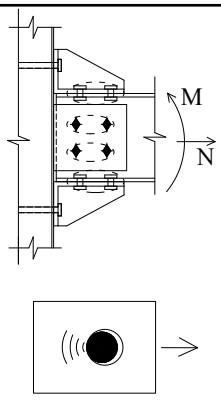	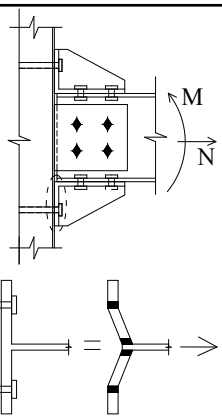	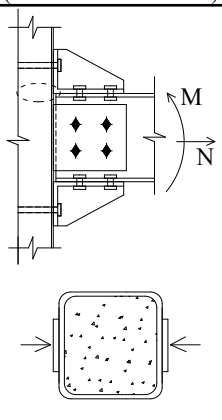

Table 6 Component assebling for initial stiffness

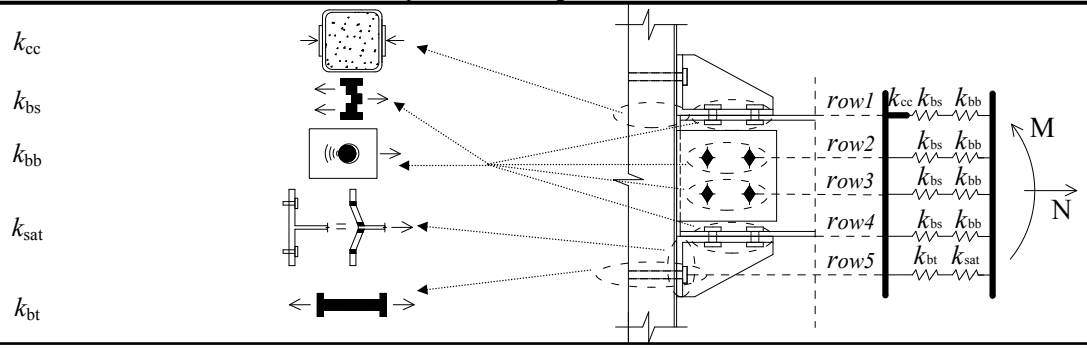

	WZ1	WZ2	WZ3
Initial stiffness of joint (model)/kNm/rad	183316(68316*)	189258(75663*)	183316(68316*)
Test initial stiffness/kNm/rad	166639	175239	178570
Model-test Differences/%	10%(-59%*)	8%(-57%*)	-3%(-39%*)

(*) means the value calculated using Eq. (6) which is not considering bolt preloading effect

Table 7 Parameters of Concrete Plastic Damage model in ABAQUS

ψ /°	ε	α_{f}	K_{c}	μ
30	0.1	1.16	0.667	0.0005

Table 8 Comparison of simulation and test results

	Load capacity/kN		Inital stiffness/kN/mm		Deformation capacity/mm	
	Test	Sim.	Test	Sim.	Test	Sim.
WZ1	124.2	116.7	2.4	2.2	180.0	204.3
WZ2	246.4	235.0	2.8	3.2	289.0	320.0
WZ3	130.9	126.5	2.5	2.3	230.0	260.0
SJS [18]	120(kNm)	126(kNm)	16386(kNm/rad)	15018(kNm/rad)	0.08(rad)	0.09(rad)